Journal Pre-proof

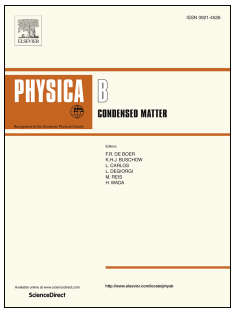

Investigation on microstructural and opto-electrical properties of Zr-doped SnO_2 thin films for Al/Zr:SnO_2/p-Si Schottky barrier diode application

K. Ravikumar, S. Agilan, M. Raja, R. Marnadu, T. Alshahrani, Mohd Shkir, M. Balaji, R. Ganesh

PII: S0921-4526(20)30455-5

DOI: https://doi.org/10.1016/j.physb.2020.412452

Reference: PHYSB 412452

To appear in: *Physica B: Physics of Condensed Matter*

Received Date: 7 July 2020

Revised Date: 5 August 2020

Accepted Date: 9 August 2020

Please cite this article as: K. Ravikumar, S. Agilan, M. Raja, R. Marnadu, T. Alshahrani, M. Shkir, M. Balaji, R. Ganesh, Investigation on microstructural and opto-electrical properties of Zr-doped SnO_2 thin films for Al/Zr:SnO_2/p-Si Schottky barrier diode application, *Physica B: Physics of Condensed Matter* (2020), doi: https://doi.org/10.1016/j.physb.2020.412452.

All the authors are contributing equally in preparation of the manuscript

Investigation on microstructural and opto-electrical properties of Zr-doped SnO_2 thin films for Al/Zr:SnO_2/p-Si Schottky barrier diode application

K. Ravikumar[1,*], S. Agilan[2], M. Raja[1], R. Marnadu[3], T. Alshahrani[4], Mohd. Shkir[5], M. Balaji[6], R. Ganesh[7]

[1]Department of Physics, Vivekanandha College of Arts and Science for Women, Tiruchengode-673205, Tamil Nadu, India
[2]Department of Physics, Coimbatore Institute of Technology, Coimbatore-641 014, Tamil Nadu, India
[3]Department of Physics, Sri Ramakrishna Mission Vidyalaya College of Arts and Science, Coimbatore-641 020, Tamil Nadu, India
[4]Department of Physics, College of Science, Princess Nourah Bint Abdulrahman University, Riyadh, 11671 Saudi Arabia
[5]Advanced Functional Materials & Optoelectronics Laboratory, Department of Physics, College of Science, King Khalid University, Abha 61413, Saudi Arabia.
[6]Department of Physics, Bannari Amman Institute of Technology, Erode-638 401, Tamil Nadu, India
[7]Department of Physics, Sri Krishna College of Technology, Coimbatore-641 042, Tamil Nadu, India

**Corresponding author: (K. Ravikumar)*
Department of Physics, Vivekanandha College of Arts and Science for Women, Tiruchengode-673205, Tamil Nadu, India
Tele/fax: +91-98432 42292,
E-mail: k.ravikumarphysics@gmail.com

Submitting author*

e-mail: shkirphysics@gmail.com

Abstract

Herein, the fabrication of novel pure and Zr-doped SnO_2 (Zr:SnO_2) films via sol-gel spin coating process for Schottky barrier diode (SBD) application has been reported. Phase and size analysis were carried out through X-ray diffraction and Scherrer rule was used to determine crystallite size, which is noticed between 2 to 7 nm. The SEM study reveals that the fabricated films contain very fine sphere-like grains. The optical transmittance of Zr:SnO_2 thin films reveals that the grown films possess high transmittance which is good for optoelectronics. The values of energy gap for all Zr:SnO_2 films were estimated between 3.90 to 3.96 eV. The dc conductivity analysis showed that SnO_2 films possess higher electrical conductivity at 8 wt.% of Zr. The barrier heights (Φ_B) and ideality factor (n) of the fabricated SBDs were calculated from both J-V and Cheung's method. Better performance was noticed for Zr (8 wt.%):SnO_2/p-Si SBD.

Keywords: Zr-doped SnO_2; optical properties; Schottky barrier diode; electrical properties, barrier height.

1. Introduction

The systems based on metal & semiconductor (MS) configuration are recognized as Schottky barrier diodes (SBDs) of MS-type. Initial work on them was reported by Schottky [1]. These structures play a very significant role in electronic devices and optoelectronic applications [2]. Interfacial layers (insulator, oxide and polymer) are implanted between metal and semiconductor to form metal-insulator/oxide/polymer-semiconductor (MIS/MOS/MPS) system of SBDs [3-5]. The quality and efficiency of MIS/MOS/MPS configurations of SBDs are reliant on numerous constraints, like fabrication of interface quality, thinness/homogeneousness, content of dopant, substrate temperature, applied voltage, series, and shunt resistances (R_s and R_{sh}), etc. [1-6]. Owing to scientific interest in electronic devices, researchers are currently focused on

improving the quality of SBDs with metal oxides, such as tin oxide (SnO_2) [7], ZnO [8], Al_2O_3 [9], WO_3 [2] and MoO3 [10]. Among them SnO_2 is an outstanding material because of its tuneable, morphological, structural and electrical properties [11].

SnO_2 is a pertinent material in many industrial and commercial applications, owing to its wide energy gap (E_g = 3.6 eV) [9], high optical transmittance, excellent electrical conductivity, high chemical & mechanical firmness than other MO transparent films [12, 13]. In general, SnO_2 belongs to the semiconductor family of n-type of large E_g in its oxygen-vacancy form and plays the role of an insulator in stoichiometric form [14]. Intrinsically undoped SnO_2 thin films have lower carrier density and mobility, hence they have low electrical conductivity [15]. Many researchers have tried to enhance the properties of the SnO_2 material through doping, annealing, and deposition techniques [16-18]. Among them, active doping is an approach to increase V_o to advance the electrical conduction behaviour of the thin films [19]. Many processes to attain the films like CVD [20], chemical bath deposition (CBD) [21], spin-coating [22] and spray pyrolysis [23] are available currently. Among these, spin coating is a better route to cast SnO_2 as well as several other advanced materials films [24-26]. It's easy to operate at low reaction temperatures, relatively inexpensive and simple deposition process to increase pinhole-free and almost fully covered surface-quality thin films [27, 28].

Several dopants, such as Cu, Zn, Mg, Ag, In, Zr, Co, Mn and Sb are incorporated with SnO_2 to enhance various properties of metal oxides [29, 30]. Among these, Zr (n-type) is a suitable dopant to obtain a good-quality interfacial layer in SBDs. Because of Sn^{4+}, its ionic radius (0.69 Å) is smaller than that of Zr^{4+}(0.72 Å). Hence, Zr^{4+} ions are substitution to Sn^{4+} ions in the crystal matrix [15, 31-33]. Therefore, Zr dopant is a very suitable dopant to enhance the properties of metal oxide-based interfacial layer in Schottky barrier diode [34]. In recent very

few reports on Zr:SnO_2 films fabrication and investigation is reported like; Zhang et al. spin-coated the Zr@SnO_2 (Zr = 0, 1, 3, 5, 7, 10 at.%) films and investigated their structure-morphology-electrical properties and noticed improved conductivity and lowermost resistivity of SnO_2 [32], Reddy et al. developed Zr@SnO_2 (Zr = 0, 1.5, 3, 4.5, and 6 at%) layer for their use in solar cell via spray pyrolysis [15], Noh et al. reported the tailoring of the electronic nature of SnO_2 NPs via Zr doping synthesized through precipitation route for competent perovskite solar cells [35]. Rammutla et al. prepared Y&Zr@SnO_2 nanocrystals via sol-gel process and inspected for structure & vibrational constraints [31], Gokulakrishnan et al. used spray pyrolysis route to prepare Zr@SnO_2 (Zr = 0 to 5 at.%) films and studied [33], Paul et al. fabricated Zr@SnO_2 (Zr = 1, 2 and 3 at.%) via sol-gel and inspected their structure & opto-electrical nature [34]. The outcomes in these reports revealed that the properties of SnO_2 are enhanced by Zr addition to its matrix. Zr also acts a major and fascinating role in altering/enhancing the key properties of several other materials like; In_2O_3, CuO, ZnO, $Bi_4Ti_3O_{12}$, TiO_2 etc. [36-40]. These reports indicate that Zr is a good element to doped in terms of improving the properties from the application's point of view. Since, the above cited reports revealed that the casting of SnO_2 films by taking 0, 2, 4, 6 and 8 wt.% $ZrCl_2$ as Zr doping agent and their Al/Zr:SnO_2/p-Si SBD via a spin-coating process has not been reported so far. Hence, here the authors aim to develop Zr:SnO_2 films and Al/Zr:SnO_2/p-Si SBD thru spin coater and inspect the consequences of Zr on structure-morphology-opto-electrical behaviour and conferred. The outcomes propose that the developed diode if useful in SBD based devices.

2. Investigational tools

2.1 Development of films

Zirconium chloride ($ZrCl_2$) in 0, 2, 4, 6 and 8 wt.% as Zr basis and 0.1 M of tin (IV) chloride pentahydrate ($SnCl_2 .5H_2O$) were taken in 5 diverse vessels containing ethanol solvent beneath the rigorous stirring at room temperature for 24 h. These final products were coated on well-eviscerated thru spin-coater functioning at 2500 rpm/30 s, and subsequently annealed for 1h at 773 K.

2.2 Device development method

Schottky barrier diode (SBDs) devices of Al/Zr:SnO_2 were fabricated on p-type silicon wafer with plane (1 0 0). The p-Si substrate was well-cleaned with H_2SO_4 and H_2O_2in the ratio of 1:2. The layer of SiO_2 from the surface of Si was detached by HF:H_2O solution in the ratio of 1:10, this was further washed by water. The above-mentioned sol-gel spin-coating process was employed for Zr:SnO_2 thin film formation on the Si wafer. The coated films annealing was done at 773 K for 1 h. Using thermal evaporation technique, aluminium (Al) was coated on the Si/Zr:SnO_2 samples with a pressure of 10^{-6} Torr [41].

3. Outcomes and Discussion

3.1. Phase authentication and microstructure studies

XRD profiles of pure SnO_2 and Zr:SnO_2 thin films are publicized in Fig. 1 obtained by employing the XRD X'PERT-PRO setup possess radiation of $CuK_{\alpha 1}$, λ = 1.54056 Å, which confirms the tetragonal crystal structure (JCPDS, No. 41-1445) [15, 42]. This result indicates that there is no significant alteration in the tetragonal crystal of SnO_2 thin film after exposure to Zr content. However, the peak intensity decreased with increasing Zr content, which shows peak broadening effect. The broad peaks signify low dimension crystallites in grown films, hence. The mean crystallites size (D) of Zr:SnO_2 films was obtained by [43, 44]:

$$D = \frac{0.89\lambda}{\beta \cos\theta} \qquad (1)$$

Values of D of Zr:SnO_2 films decreased with rising the Zr content in it, in which in the range of 5.13 - 2.2 nm. Noh et al, also observed the D value for pure ~ 2.69 ± 0.39 and for Zr@SnO_2 ~ 2.17 ± 0.64 nm [35]. Zhang et al. reported the D values between 10 to 8 nm when Zr is doped in SnO_2. Reddy et al. notice the D reduction of SnO_2 when doped with Zr [32]. Further, by eqs. (2-4) [42] , the no. of dislocations (δ), strain (ε) and fault of stacking (SF) of pure SnO_2 and Zr:SnO_2 films were estimated and given in Table 1.

$$\delta = \frac{1}{D^2} \quad (2)$$

$$\varepsilon = \frac{\lambda}{D \sin\theta} - \frac{\beta}{\tan\theta} \quad (3)$$

$$SF = \left[\frac{2\pi^2}{45(3\tan\theta)^{\frac{1}{2}}}\right]\beta \quad (4)$$

The calculated values of the defect factors decreased with higher concentration of Zr. SnO_2 film with 8 wt.% of Zr show a δ, ε and SF values ~ 0.63 x 10^{17} lines/m^2, 0.87 x 10^{-3} lines/m^2, 1.975, respectively. This confirms that the Zr-incorporated SnO_2 thin films reduce the defect factors.

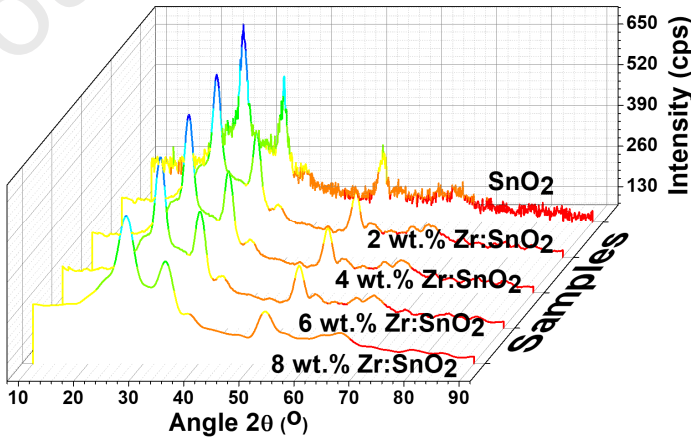

Fig. 1 XRD of SnO_2 thin films with various concentrations of Zr dopant.

Table 1: Structural properties of SnO_2 thin films with various concentrations of Zr dopant.

Zr in Wt.%	2θ (º)	d (Å)	h k l	FWHM (radians)	D (nm)	$\delta\times10^{17}$ lines/m^2	$\varepsilon\times10^{-2}$ lines/m^2	$SF\times10^{-2}$
0	26.6846	4.484	111	3.34	3.18	0.989	1.090	2.415
	33.855	4.187	101	2.65	3.46	0.833	1.001	2.605
	51.83	3.407	211	1.76	4.53	0.480	0.766	2.919
2	27.014	3.300	110	5.12	2.75	1.321	1.250	2.782
	34.27	2.616	101	4.86	2.95	1.147	1.162	3.049
	52.244	1.751	211	3.64	4.19	0.568	0.817	3.144
4	27.222	3.275	110	3.10	4.54	0.485	0.755	1.693
	34.488	2.600	101	3.63	3.95	0.641	0.868	2.290
	52.484	1.743	211	2.32	6.57	0.231	0.522	2.017
6	27.604	3.231	111	3.04	4.63	0.465	0.740	1.673
	34.871	2.572	101	3.63	3.95	0.640	0.867	2.307
	52.954	1.729	211	3.64	4.20	0.561	0.815	3.185
8	27.725	3.217	111	3.58	3.94	0.644	0.871	1.975
	34.991	2.564	101	3.32	4.32	0.535	0.794	2.115
	52.834	1.732	211	2.93	5.21	0.368	0.658	2.563

3.2 Morphological study

Fig. 2 demonstrates the FE-SEM (Model: JEOL JEM 2100) images of different concentrations of Zr-incorporated SnO_2thin films. Regular-shaped sphere-like grains with rough surface morphology were observed in SnO_2 films as uncovered in Fig. 2(a). Grain size was slightly reduced in the case of 2 wt.% of Zr:SnO_2thin film surfaces (Fig. 2(b)). Figure 2(c) shows that the grain size of 4 wt.% of Zr:SnO_2 film was further decreased. In higher doping concentrations of 6 and 8 wt.% of Zr:SnO_2, very fine nano-sized grains were detected as shown in Fig. 2(d)-(e). This directs that the Zr content strongly interrupts the grain growth and density of SnO_2 films. FESEM images revealed that the grown films possess compact nanograins at higher Zr contents. Increasing doping content can increase stress in the SnO_2 grains, which will disturb the grain growth process and decrease the nucleation agent in the system [15]. Reddy et

al. also observed same type of grain size lessening on 1.5, 3.0. 4.5 and 6 at.% Zr content addition to SnO_2 films readied by Spray process [15].

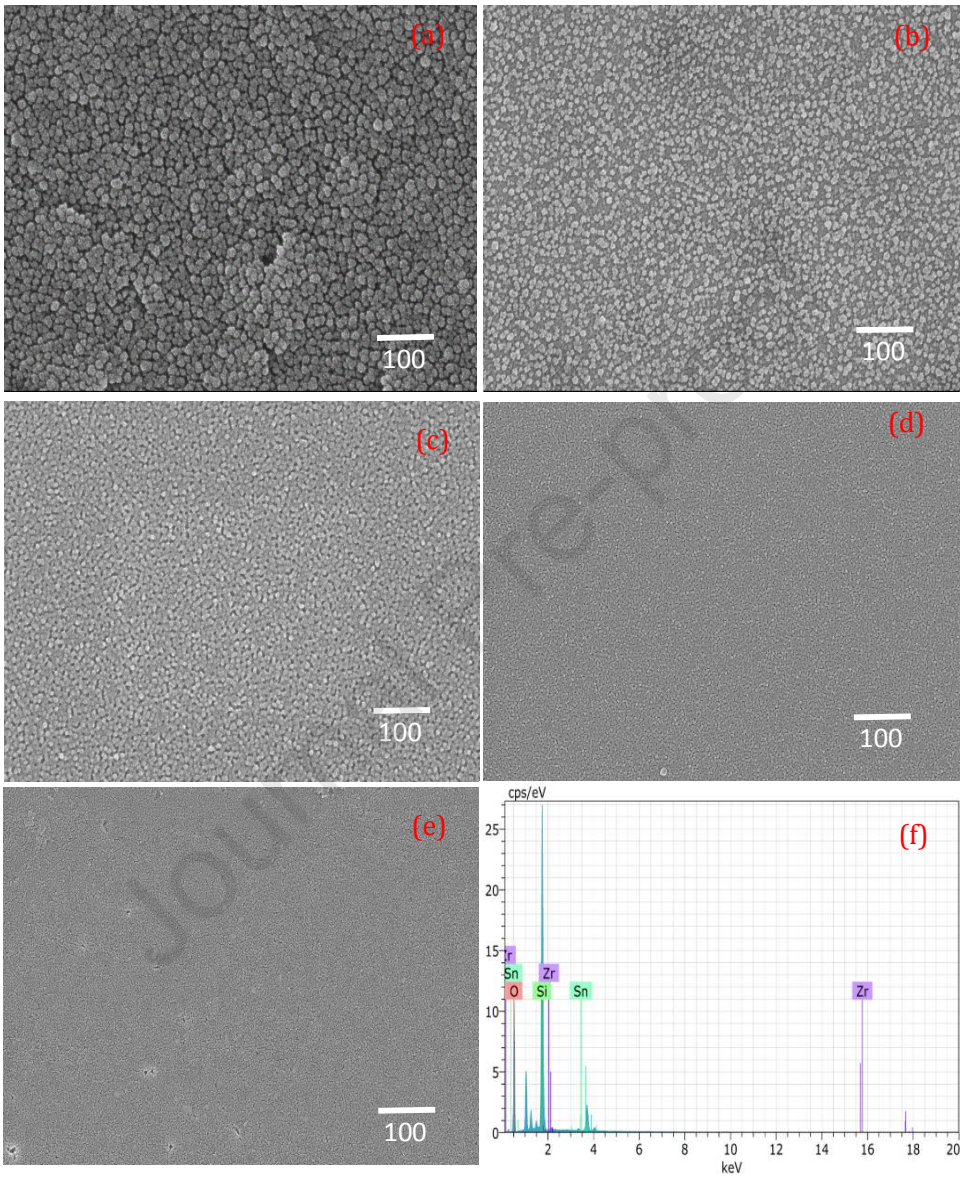

Fig. 2 FE-SEM images of SnO_2 thin films with different concentration of Zr. (a) SnO_2, (b) Zr(2 wt.%):SnO_2, (c) Zr(4 wt.%):SnO_2, (d) Zr(6 wt.%):SnO_2, (e) Zr(8 wt.%):SnO_2 and (f) EDAX spectra of Zr(8 wt.%):SnO_2 thin film.

3.2 Evaluation of energy gap (E_g)

Fig. 3 (a) & (b) displays the optical absorption and transmittance density profiles of Zr:SnO_2 films over the wavelength region of 300–900 nm recorded via Lambda 35 UV-Vis spectrometer. It shows that the absorption/transmittance value of Zr:SnO_2 is larger compared to SnO_2 films in the visible region of 355–530 nm is owing to the densification of the grain growth in the latter [45]. A minute non-systematic shifting is visible in absorbance of films with Zr doping. The films are noticed to have good transmittance values viz. ~ 67% (see fig. 3(b)) and low absorbance (see fig. 3(a). A higher optical absorption is noticed for SnO_2 films doped with 2 wt.%. To inveterate the Zr impact on E_g value of SnO_2, the Tauc's relation is used [46, 47]:

$$(\alpha h\nu)^m = A\left(h\nu - E_g\right) \qquad (5)$$

here symbols are well-recognized [48] and transition m is 2 for SnO_2 semiconductors. Here, coefficient to absorption (α) was obtained by [49]:

$$\alpha = \left(2.303\,\frac{\text{Absorbance}}{\text{thickness}}\right) \qquad (6)$$

The optical E_g of SnO_2 and Zr:SnO_2 films was obtained from plot of Tauc's as revealed in Fig. 3(c). Alteration in values of E_g w.r.t. Zr content can be assessed thru straight section of graph extrapolation with bandgap energy axis. It can be seen that the value of E_g lies between 3.90 from 3.96 eV for Zr concentration from 2 to 8 wt. % and the highest value was noticed for 8 wt.% Zr:SnO_2 film this might be due to increasing defects and lower density of localized states in ZrO_2 thin films. The Eg values are in accord with SnO_2 which are lied between 3.6 to 4.0 eV [35]. Such E_g alteration in SnO_2 thru Zr contents doping was also noticed by Zhang et al. and observed between 3.88 to 3.95 eV [32], Reddy et al. noticed the lessening of E_g from 3.94 to 3.68 eV on doping of Zr into sprayed SnO_2 films from 1.5 to 6.0 wt.% [15] etc. The inter-CB absorption absence is a owe to key features of SnO_2 band assembly, establishing as a great inner gap within the CB which eradicates transitions in Vis region [50, 51]. According to Moss–

Burstein shift, generation of more conduction electrons pushes the Fermi level to higher energy. These E_g values are in correlation to prior documented ones [52].

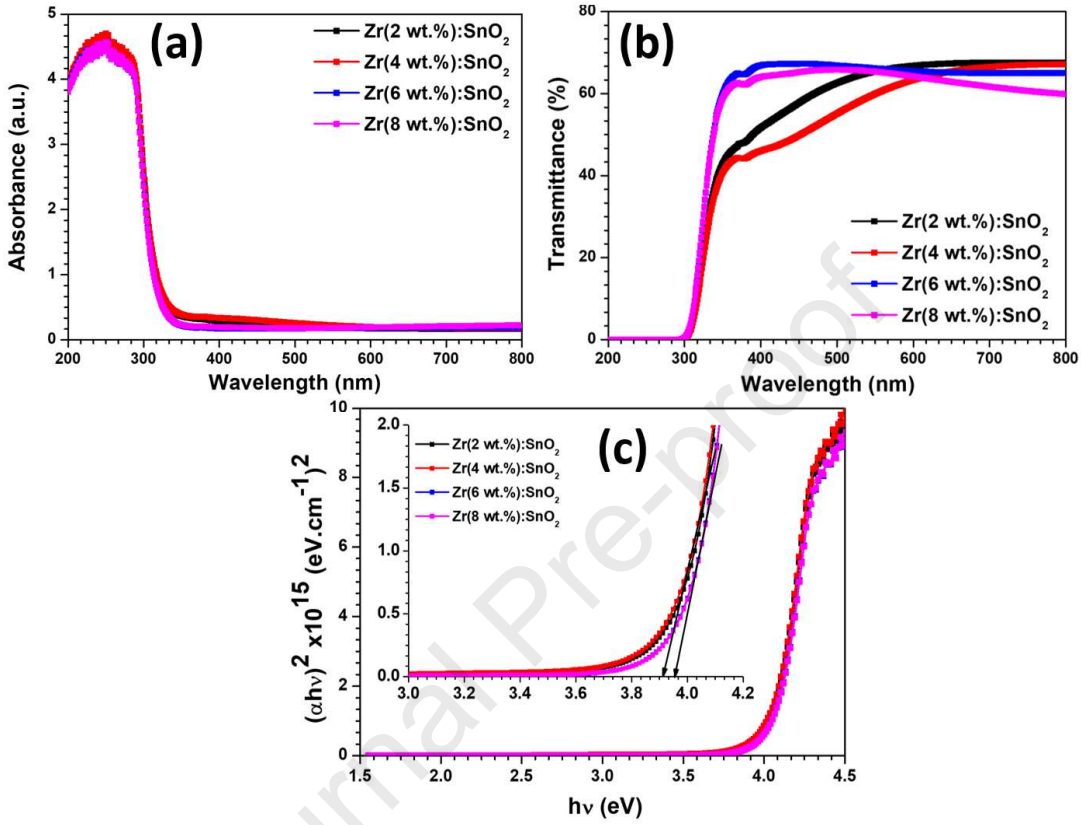

Fig. 3 (a) Optical absorbance spectra, (b) Transmittance spectra and (b) Tauc's $[(\alpha h\nu)^{1/2}$ vs. $h\nu]$ plot of Zr:SnO_2 thin films.

3.3 Direct current (dc) electrical study

Electrical analysis of different concentrations of Zr-doped SnO_2 films was done over the 303-473K temperature region using two probe methods (Keithley source meter Model: 6517-B). Fig. 4 shows the nature of conductivity of dc (σ_{dc}) for Zr:SnO_2 films, the graph revealed that the σ_{dc} is rising with rise of temperature as well as Zr content in SnO_2. The 8.0 wt.% of Zr-doped SnO_2 film has higher electrical conducting nature owing to Zr^{4+} ions in the Sn^{4+} and O^{2-} ions, which create trap centres in the SnO_2 lattice [53]. This generates new mobile electrons in SnO_2 lattice, which raise the electrical conductivity to 303 K. At room temperature, pure and 8 wt.% of

Zr-doped SnO_2 thin films with corresponding σ_{dc} values are 6.80 x 10^{-11} and 5.41 x 10^{-6}, respectively. The Arrhenius equation (σ_{dc}) is expressed as [54]:

$$\sigma = \sigma_0 \exp\left(\frac{-Ea}{K_B T}\right) \qquad (7)$$

here E_a stand for energy of activation, and the other sign are recognized well [55]. The role of temperature in Zr:SnO_2 films is publicized in Fig. 5. The ln(σ_{dc}) vs 1/T plot (see Fig. 5) was linearly fit to straight line indicates that the activation energy decreased with temperature.

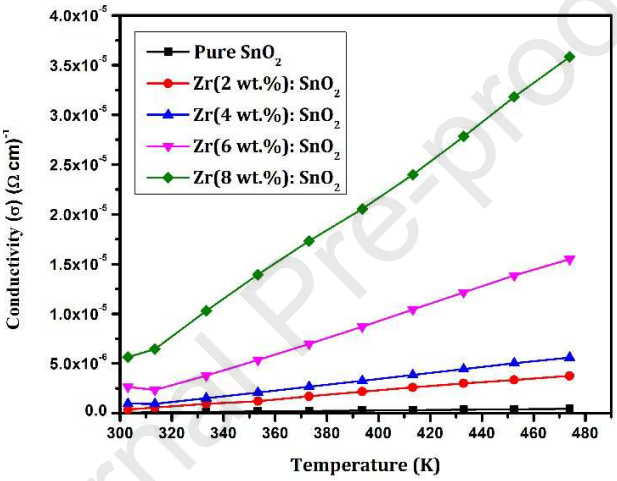

Fig. 4 Temperature dependence of electrical conductivity of the Zr-doped SnO_2 thin films. (a) SnO_2, (b) Zr(2 wt.%):SnO_2, (c) Zr(4 wt.%):SnO_2 and (d) Zr(6 wt.%):SnO_2.

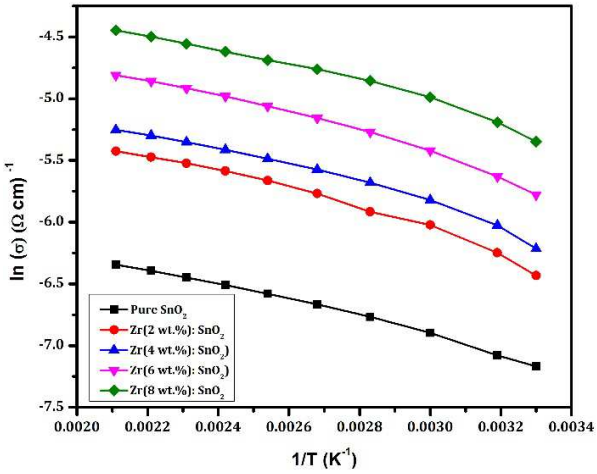

Fig. 5 Plot of ln(σ_{dc}) vs. 1/T of the SnO_2 thin films for different dopant concentration of Zr. (a) SnO_2, (b) Zr(2 wt.%):SnO_2, (c) Zr(4 wt.%):SnO_2 and (d) Zr(6 wt.%):SnO_2.

3.5 SBD study

The I vs. V values of different concentrations of Zr-doped Al/Zr-SnO_2/p-Si SBDs were executed beneath the dark state at 303 K using a Keithley source meter (6517-B). The total I of SBD is stated as [56, 57]:

$$I = I_0 \left[\exp\left(\frac{qV}{nk_BT}\right) - 1\right] \quad (8)$$

where V, I, I_0, q and T are the applied voltage between −3V & +3V, current, drip current at V=0, charge (1.602 x 10^{-19} C) and temperature [58]:

$$I_0 = AA^*T^2\exp\left(\frac{-q\Phi_B}{k_BT}\right) \quad (9)$$

The ideality factor (n) has been expressed by:

$$n = \frac{q}{k_BT}\left(\frac{dV}{d\ln(I)}\right) \quad (10)$$

Barrier height (Φ_B) was identified by relation:

$$\Phi_B = \frac{k_BT}{q}\ln\left(\frac{A^*T^2}{I_0}\right) \quad (11)$$

here A^* stand for effective Richardson constraint for p-Si. The estimated n and Φ_B along with I_o values are given in Table 3 and noticed to rise and decline, correspondingly with rising the Zr content in SnO_2. Also the reverse saturation current value is lessening from 1.652 to 1.050 nA on rising of Zr into SnO_2 matrix. By putting the developed device in dark the ln(I)-V study was carried out for different Zr content fused Al/Zr:SnO_2/p-Si diode as presented in Fig. 6. Device ideality (n) improves from 3.21 to 2.78 of Al/Zr:SnO_2/p-Si diode compared to Al/SnO_2/p-Si. As the n value is > 2 indicates charge carriers of higher recombining centers in over dynamic region. The value of ideality factor is dependent on the applied bias voltage, barrier inhomogeneity as

well as surface states, depletion layer width, dielectric value of interfacial layer, and the thickness of interfacial layer. A thin Zr:SiO_2 layer at interface affects the recombination of charge in the region of space charge, their non-uniformity & layer thickness may be the cause of getting larger n values of the device [59, 60].

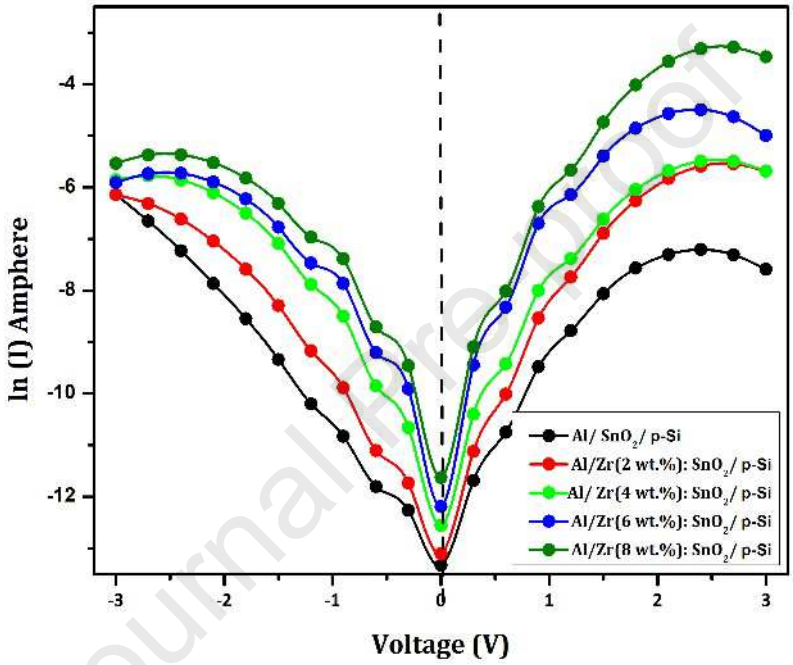

Fig. 6 Plot of ln(I) vs. V of the SnO_2 thin films for various dopants of Zr in the Al/Zr:SnO_2/p-Si.

Fig. 7 shows the metal-semiconductor contacts of the SBDs for a) Before contact b) Thermal equilibrium after contact c) under forward bias d) under negative bias condition e) Energy level diagram of Al/Zr:SnO_2/p-Si diode. In thermal equilibrium (Fig. 7b), for the carriers, the apparent barrier height (BH) from metal to semiconductor is higher than semiconductor to metal. Therefore, the value of BH calculated from forward bias I-V measurement is always lower than the reverse bias C-V measurements (from C^{-2} vs V plot). When metal and semiconductor contacted, the majority holes in p-Si passed the front of metal and similarly electrons passed the front of p-Si until their Fermi energy level becomes same level. In this way, the interior electric

field occurs from metal to semiconductor. After that both the conductance and VB become curvature towards upside but the energy band of semiconductor unchanged with decreasing of acceptor atoms (N_A) (E_F = kT/q.Ln (N_V/N_A)). Under forward bias (Fig. 7 c), interior and external electric field has opposite direction and so total electric field decreases. But, under reverse bias both interior and external electric field are in the same direction and so the total electric field is higher than the forward bias region**.**

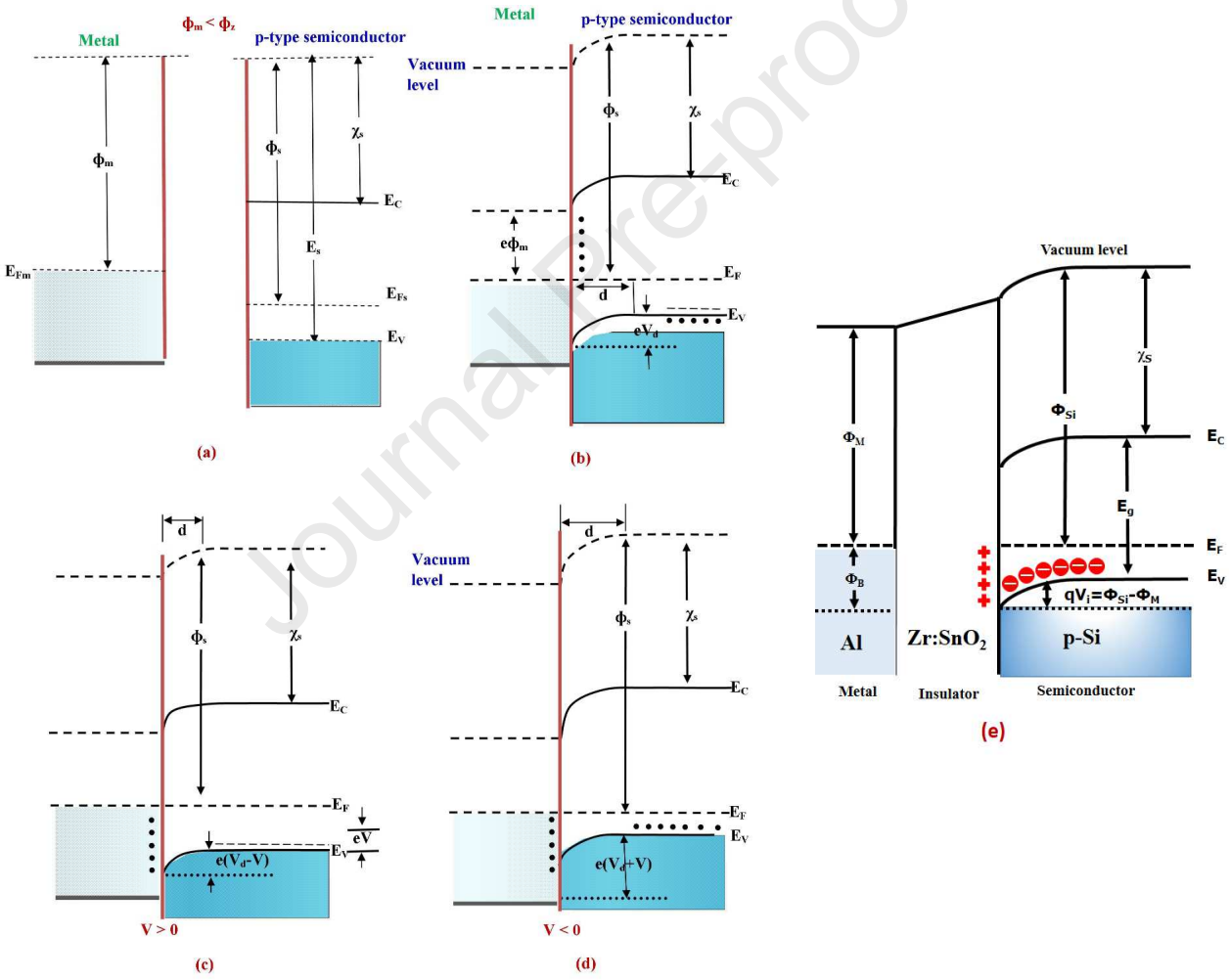

Fig. 7. Metal-p-type semiconductor contact a) Before contact, b) Thermal equilibrium after contact c) under forward bias d) under negative bias conditions (e) Energy level diagram of Al/Zr:SnO_2/p-Si diode.

The calculated Φ_B of the fabricated SBDs have been increased from 0.855 to 0.96 eV. This improvement in values of Φ_B is might be owed to that electrons at large scale own plentiful energy to overcome the barrier in Zr:SnO_2 films. Better performance was achieved at 8 wt.% of Zr content in Zr:SnO_2/p-Si SBD. I_0 decreases with Zr content in the SnO_2 thin film and signify trapping of electrons at the boundaries of grains which are accumulated through doping ions. Reduction of barrier height (Φ_B) with the incorporation of doping content is credited to improved charge carrier, which increases the Fermi level and lowers the barrier height [61-64]. Further, the values of series resistance (R_s), n and Φ_B evaluated from I-V data using Cheung's equations. Generally, J-V method is applied to the linear region at low bias region of the ln(I)–V characteristics, whereas Cheung's function is applied non-linear region in the high bias region of the ln(I)–V characteristics. It is defined by the following relations [65-69]:

$$\frac{dV}{dln(I)} = jR_s + n\left(\frac{KT}{q}\right) \quad (12)$$

$$H(I) = V - n\left(\frac{KT}{q}\right)\ln\left(\frac{j}{A^*T^2}\right) \quad (13)$$

$$H(I) = JR_s + n\Phi_B \quad (14)$$

Fig. 8(a) displays a plot of dV/dIn(I) versus I for different Zr concentration of SnO_2 thin films. Form the Eqn.(12), the series resistance (R_s) and ideality factor (n) values can be identified by linear region of the plot fitted on the slope value and nk_BT/q as the y-axis intercept values. A plot of H(I) vs. I (Fig. 8(b)) yields n and Φ_B as the intercept on the y axis and the second determination of R_S as the slope (using Eqn. (14)). From H(I) versus I, the Φ_B and R_S values are reported in Table. 2. Interestingly, the n and Φ_B remain almost the same or slightly varies with Zr concentration of SnO_2 compared to the I-V method. The series resistance values are calculated using the plots of dV/dln(I) Vs I and H(I) Vs I. The Zr influences on the series resistance values. The resistance values are given in Table. 2. It is noted that the Zr concentration increases from 2

to 8 wt.% the resistance value varied from 8.45 to 6.25 (KΩ cm). Moreover, the series resistance value decreases for Zr concentration device for each device.

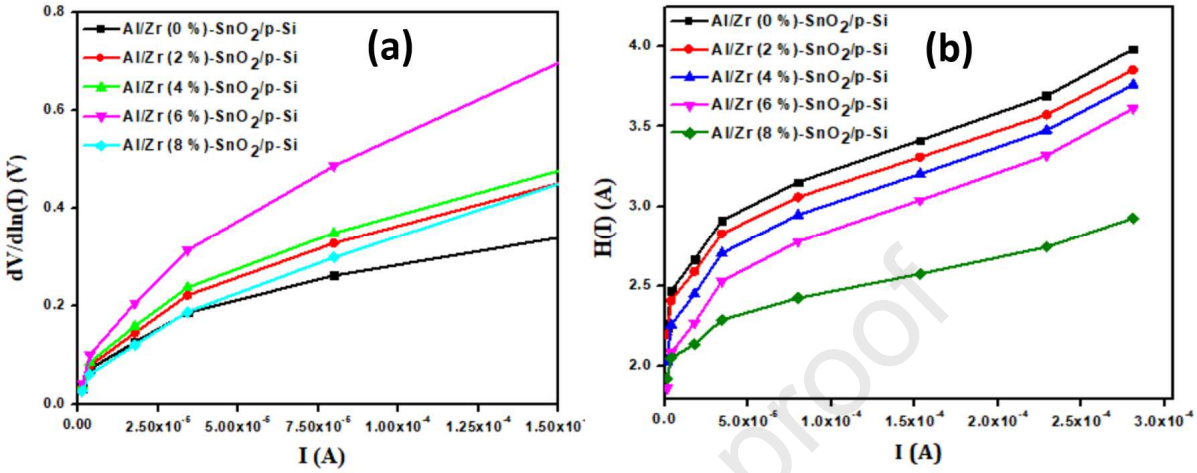

Fig. 8 (a) plot of dV/dIn(I) versus I and (b) H(I) versus I for various dopants of Zr.

Table 2 Calculated values of series resistance (Rs), n and Φ_B from I-V data using Cheung's equations.

Device Structure	Reverse saturation Current (I_o) in nA	Barrier Height (Φ_B) eV		Ideality factor (n)		Series resistance (R_s) (KΩ cm)	
		I-V	Cheung's	I-V	Cheung's	dV/dln(I)	H(I)
Al/SnO_2/p-Si	1.652	0.73	0.74	3.21	3.19	8.45	8.98
Al/2 wt. % of Zr:SnO_2/p-Si	1.583	0.77	0.79	3.21	3.195	7.98	8.84
Al/4 wt. % of Zr:SnO_2/p-Si	1.402	0.83	0.84	3.01	2.99	7.55	8.21
Al/6 wt. % of Zr:SnO_2/p-Si	1.208	0.89	0.93	2.85	2.80	6.34	7.65
Al/8 wt. % of Zr:SnO_2/p-Si	1.050	0.96	0.98	2.78	2.76	6.25	7.24

4. Conclusion

Different Zr concentrations added SnO_2 films were facilely accomplished thru sol-gel spin coater processing and characterized for Zr:SnO_2/p-Si SBDs. XRD analysis reveals is no transformation in the tetragonal crystal system SnO_2 thin film; even Zr(8 wt.%):SnO_2 thin films exhibited better performance as Al/Zr:SnO_2/p-Si SBDs. The Scherrer rule was employed to determine crystallite size and noticed between 2 to 5 nm. FE-SEM analysis indicates that Zr content strongly interrupts the growth of grains and enhance the compactness/density of SnO_2 films. The low absorbance/high transmittance indicates goof quality films for applications in optoelectronic. The energy gap was estimated between 3.90 to 3.96 eV for Zr:SnO_2 films. The Zr:SnO_2 films with 8 wt.% of Zr have higher electrical conductivity ~ 7.8 $x10^{-7}$ Ω^{-1} cm^{-1} as shown by dc electrical study. The ideality factor value of the fabricated SBDs was noticed between 3.21-2.78 and barrier heights (Φ_B) of the fabricated SBDs increased from 0.855 to 0.96 eV. The values of n and Φ_B evaluated from Cheung's equations is comparably better than J-V method. The 8 wt.% of SBDs exhibited a minimum value of series resistance in both dV/dln(I) and H(I) vs. I. From all the above results, it could be concluded that the fabricated MIS diodes are highly appropriate for optoelectronic application.

Acknowledgements

Author T. Alshahrani would like to express her gratitude to Deanship of Scientific Research at Princess Nourah bint Abdulrahman University for funding this research through the Fast-track Research Funding Program. Author M. Shkir would like to express his gratitude to King Khalid University, Saudi Arabia for providing administrative and technical support.

Declaration of Competing Interest

The authors declared that there is no conflict of interest.

References

[1] Ç. Bilkan, Y. Badali, S. Fotouhi-Shablou, Y. Azizian-Kalandaragh, Ş. Altındal, On the temperature dependent current transport mechanisms and barrier inhomogeneity in Au/SnO2–PVA/n-Si Schottky barrier diodes, Applied Physics A, 123 (2017) 560.
[2] Y. Liu, W.M. Tang, P.T. Lai, A comparative study of Hf and Ta incorporations in the dielectric of Pd-WO3-SiC Schottky-diode hydrogen sensor, Sensors and Actuators B: Chemical, 259 (2018) 725-729.
[3] K. Ravikumar, S. Agilan, N. Muthukumarasamy, M. Raja, R. Lakshmanan, R. Ganesh, Influence of Annealing Temperature on Structural and dc Electrical Properties of SnO2 Thin Films for Schottky Barrier Diodes, Silicon, 10 (2018) 1591-1599.
[4] Y. Kobayashi, H. Ishimori, A. Kinoshita, T. Kojima, M. Takei, H. Kimura, S. Harada, Evaluation of Schottky barrier height on 4H-SiC m-face $\{ 1\bar{1}00\} $ for Schottky barrier diode wall integrated trench MOSFET, Japanese Journal of Applied Physics, 56 (2017) 04CR08.
[5] L.W. Lim, F. Aziz, F.F. Muhammad, A. Supangat, K. Sulaiman, Electrical properties of Al/PTB7-Th/n-Si metal-polymer-semiconductor Schottky barrier diode, Synthetic Metals, 221 (2016) 169-175.
[6] A. Kurtz, E. Muñoz, J. Chauveau, A. Hierro, Deep-level spectroscopy in metal–insulator–semiconductor structures, Journal of Physics D: Applied Physics, 50 (2017) 065104.
[7] G.T. Dang, T. Uchida, T. Kawaharamura, M. Furuta, A.R. Hyndman, R. Martinez, S. Fujita, R.J. Reeves, M.W. Allen, Silver oxide Schottky contacts and metal semiconductor field-effect transistors on SnO2thin films, Applied Physics Express, 9 (2016) 041101.
[8] L.J. Brillson, Y. Lu, ZnO Schottky barriers and Ohmic contacts, Journal of Applied Physics, 109 (2011) 8.
[9] M. Sharma, S.K. Tripathi, Frequency and voltage dependence of admittance characteristics of Al/Al2O3/PVA:n-ZnSe Schottky barrier diodes, Materials Science in Semiconductor Processing, 41 (2016) 155-161.
[10] J. Chen, J. Lv, Q. Wang, Electronic properties of Al/MoO3/p-InP enhanced Schottky barrier contacts, Thin Solid Films, 616 (2016) 145-150.
[11] Y. Son, J. Li, R.L. Peterson, In Situ Chemical Modification of Schottky Barrier in Solution-Processed Zinc Tin Oxide Diode, ACS Applied Materials & Interfaces, 8 (2016) 23801-23809.
[12] K. Bouras, G. Schmerber, H. Rinnert, D. Aureau, H. Park, G. Ferblantier, S. Colis, T. Fix, C. Park, W.K. Kim, Structural, optical and electrical properties of Nd-doped SnO2 thin films fabricated by reactive magnetron sputtering for solar cell devices, Solar energy materials and solar cells, 145 (2016) 134-141.
[13] W. Ben Haj Othmen, Z. Ben Hamed, B. Sieber, A. Addad, H. Elhouichet, R. Boukherroub, Structural and optical characterization of p-type highly Fe-doped SnO2 thin films and tunneling transport on SnO2:Fe/p-Si heterojunction, Applied Surface Science, 434 (2018) 879-890.
[14] E. Boyalı, V. Baran, T. Asar, S. Özçelik, M. Kasap, Temperature dependent electron transport properties of degenerate SnO2 thin films, Journal of Alloys and Compounds, 692 (2017) 119-123.
[15] N.N.K. Reddy, H.S. Akkera, M.C. Sekhar, S.-H. Park, Zr-doped SnO 2 thin films synthesized by spray pyrolysis technique for barrier layers in solar cells, Applied Physics A, 123 (2017) 761.
[16] R. Singh, M. Kumar, S. Shankar, R. Singh, A.K. Ghosh, O.P. Thakur, B. Das, Effects of Sb, Zn doping on structural, electrical and optical properties of SnO2 thin films, Materials Science in Semiconductor Processing, 31 (2015) 310-314.
[17] N. Van Toan, N. Viet Chien, N. Van Duy, H. Si Hong, H. Nguyen, N. Duc Hoa, N. Van Hieu, Fabrication of highly sensitive and selective H2 gas sensor based on SnO2 thin film sensitized with microsized Pd islands, Journal of Hazardous Materials, 301 (2016) 433-442.
[18] B. Thomas, B. Skariah, Spray deposited Mg-doped SnO2 thin film LPG sensor: XPS and EDX analysis in relation to deposition temperature and doping, Journal of Alloys and Compounds, 625 (2015) 231-240.
[19] B.W. Veal, S.K. Kim, P. Zapol, H. Iddir, P.M. Baldo, J.A. Eastman, Interfacial control of oxygen vacancy doping and electrical conduction in thin film oxide heterostructures, Nature communications, 7 (2016) 1-8.
[20] Y.M. Lu, J. Jiang, C. Xia, B. Kramm, A. Polity, Y.B. He, P.J. Klar, B.K. Meyer, The influence of oxygen flow rate on properties of SnO2 thin films grown epitaxially on c-sapphire by chemical vapor deposition, Thin Solid Films, 594 (2015) 270-276.

[21] B. Opasanont, K.T. Van, A.G. Kuba, K.R. Choudhury, J.B. Baxter, Adherent and Conformal Zn(S,O,OH) Thin Films by Rapid Chemical Bath Deposition with Hexamethylenetetramine Additive, ACS Applied Materials & Interfaces, 7 (2015) 11516-11525.
[22] K. Ravikumar, S. Agilan, M. Raja, L. Raja, B. Gokul, R. Ganesh, N. Muthukumarasamy, Design and fabrication of Al/Sr:SnO2/p-Si schottky barrier diode based on strontium-doped SnO2 thin film, Materials Research Express, 6 (2018) 026413.
[23] M. Balaji, J. Chandrasekaran, M. Raja, Role of substrate temperature on MoO3 thin films by the JNS pyrolysis technique for P–N junction diode application, Materials Science in Semiconductor Processing, 43 (2016) 104-113.
[24] M. Shkir, A. Khan, A.A. Ansari, A.M. El-Toni, I.S. Yahia, M.A. Khan, H. Algarni, S. AlFaify, Facilely fabricated Dy:PbI2/glass thin films and their structural, linear and nonlinear optical studies for opto-nonlinear applications, Vacuum, 173 (2020) 109122.
[25] M. Shkir, M.T. Khan, S. AlFaify, Novel Nd-doping effect on structural, morphological, optical, and electrical properties of facilely fabricated PbI2 thin films applicable to optoelectronic devices, Applied Nanoscience, 9 (2019) 1417-1426.
[26] M. Shkir, S. AlFaify, Effect of Gd3+ doping on structural, morphological, optical, dielectric, and nonlinear optical properties of high-quality PbI2 thin films for optoelectronic applications, Journal of materials research, 34 (2019) 2765-2774.
[27] L.P. Ravaro, L.V.A. Scalvi, M.H. Boratto, Improved electrical transport in lightly Er-doped sol–gel spin-coating SnO2 thin films, processed by photolithography, Applied Physics A, 118 (2015) 1419-1427.
[28] M. Shkir, A. Khan, A.M. El-Toni, A. Aldalbahi, I.S. Yahia, S. AlFaify, Structural, morphological, opto-nonlinear-limiting studies on Dy:PbI2/FTO thin films derived facilely by spin coating technique for optoelectronic technology, Journal of Physics and Chemistry of Solids, 130 (2019) 189-196.
[29] H.S. Oh, H.N. Nong, P. Strasser, Preparation of mesoporous Sb‐, F‐, and In‐doped SnO2 bulk powder with high surface area for use as catalyst supports in electrolytic cells, Advanced Functional Materials, 25 (2015) 1074-1081.
[30] P. Nithyadharseni, K.P. Abhilash, S. Petnikota, M.R. Anilkumar, R. Jose, K.I. Ozoemena, R. Vijayaraghavan, P. Kulkarni, G. Balakrishna, B.V.R. Chowdari, S. Adams, M.V. Reddy, Synthesis and Lithium Storage Properties of Zn, Co and Mg doped SnO2 Nano Materials, Electrochimica Acta, 247 (2017) 358-370.
[31] K.E. Rammutla, A.V. Chadwick, J. Harding, D.C. Sayle, R.M. Erasmus, EXAFS and Raman scattering studies of Y and Zr doped nano-crystalline tin oxide, Journal of Physics: Conference Series, 249 (2010) 012054.
[32] X. Zhang, X. Liu, H. Ning, W. Yuan, Y. Deng, X. Zhang, S. Wang, J. Wang, R. Yao, J. Peng, Characterization studies of the structure and properties of Zr-doped SnO2 thin films by spin-coating technique, Superlattices and Microstructures, 123 (2018) 330-337.
[33] V. Gokulakrishnan, S. Parthiban, K. Jeganathan, K. Ramamurthi, Investigation on the effect of Zr doping in ZnO thin films by spray pyrolysis, Applied Surface Science, 257 (2011) 9068-9072.
[34] G.K. Paul, S. Bandyopadhyay, S.K. Sen, S. Sen, Structural, optical and electrical studies on sol–gel deposited Zr doped ZnO films, Materials Chemistry and Physics, 79 (2003) 71-75.
[35] Y.W. Noh, J.H. Lee, I.S. Jin, S.H. Park, J.W. Jung, Tailored electronic properties of Zr-doped SnO2 nanoparticles for efficient planar perovskite solar cells with marginal hysteresis, Nano Energy, 65 (2019) 104014.
[36] H. Kim, J. Horwitz, G. Kushto, S. Qadri, Z. Kafafi, D. Chrisey, Transparent conducting Zr-doped In 2 O 3 thin films for organic light-emitting diodes, Applied Physics Letters, 78 (2001) 1050-1052.
[37] H. Mersian, M. Alizadeh, N. Hadi, Synthesis of zirconium doped copper oxide (CuO) nanoparticles by the Pechini route and investigation of their structural and antibacterial properties, Ceramics International, 44 (2018) 20399-20408.
[38] H. Kim, J. Horwitz, W. Kim, S. Qadri, Z. Kafafi, Anode material based on Zr-doped ZnO thin films for organic light-emitting diodes, Applied physics letters, 83 (2003) 3809-3811.
[39] J. Chen, Q. Yun, W. Gao, Y. Bai, C. Nie, S. Zhao, Improved ferroelectric and fatigue properties in Zr doped Bi4Ti3O12 thin films, Materials Letters, 136 (2014) 11-14.
[40] A. Juma, I. Oja Acik, A.T. Oluwabi, A. Mere, V. Mikli, M. Danilson, M. Krunks, Zirconium doped TiO2 thin films deposited by chemical spray pyrolysis, Applied Surface Science, 387 (2016) 539-545.
[41] M. Raja, J. Chandrasekaran, M. Balaji, Evaluation of microstructural and electrical properties of WO3-x thin films for p-Si/n-WO3-x/Ag junction diodes, Optik, 127 (2016) 11009-11019.
[42] M. Raja, J. Chandrasekaran, M. Balaji, B. Janarthanan, Impact of annealing treatment on structural and dc electrical properties of spin coated tungsten trioxide thin films for Si/WO3/Ag junction diode, Materials Science in Semiconductor Processing, 56 (2016) 145-154.
[43] A. Patterson, The Scherrer formula for X-ray particle size determination, Physical review, 56 (1939) 978.

[44] M. Shkir, S. AlFaify, Tailoring the structural, morphological, optical and dielectric properties of lead iodide through Nd3+ doping, Scientific Reports, 7 (2017) 16091.
[45] B. Cullity, S. Stock, Elements of X-Ray Diffraction Third edition Prentice Hall Upper Saddle River, in, NJ, 2001.
[46] R. Brahma, M.G. Krishna, A. Bhatnagar, Optical, structural and electrical properties of Mn doped tin oxide thin films, Bulletin of Materials Science, 29 (2006) 317-322.
[47] M. Shakir, S. Kushwaha, K. Maurya, G. Bhagavannarayana, M. Wahab, Characterization of ZnSe nanoparticles synthesized by microwave heating process, Solid State Communications, 149 (2009) 2047-2049.
[48] M. Shkir, S. Aarya, R. Singh, M. Arora, G. Bhagavannarayana, T. Senguttuvan, Synthesis of ZnTe Nanoparticles by Microwave Irradiation Technique, and Their Characterization, Nanoscience and Nanotechnology Letters, 4 (2012) 405-408.
[49] M.A. Manthrammel, M. Shkir, M. Anis, S. Shaikh, H.E. Ali, S. AlFaify, Facile spray pyrolysis fabrication of Al: CdS thin films and their key linear and third order nonlinear optical analysis for optoelectronic applications, Optical Materials, 100 (2020) 109696.
[50] J. Tauc, Optical properties and electronic structure of amorphous Ge and Si, Materials Research Bulletin, 3 (1968) 37-46.
[51] X. Chang, S. Sun, X. Xu, Z. Li, Synthesis of transition metal-doped tungsten oxide nanostructures and their optical properties, Materials Letters, 65 (2011) 1710-1712.
[52] J.C. Inkson, The Normal System, in: Many-Body Theory of Solids, Springer, 1984, pp. 183-217.
[53] M. Regragui, V. Jousseaume, M. Addou, A. Outzourhit, J. Bernede, B. El Idrissi, Electrical and optical properties of WO3 thin films, Thin Solid Films, 397 (2001) 238-243.
[54] M. Zubair Ansari, N. Khare, Thermally activated band conduction and variable range hopping conduction in Cu2ZnSnS4 thin films, Journal of Applied Physics, 117 (2015) 025706.
[55] R. Marnadu, J. Chandrasekaran, M. Raja, M. Balaji, V. Balasubramani, Impact of Zr content on multiphase zirconium–tungsten oxide (Zr–WOx) films and its MIS structure of Cu/Zr–WOx/p-Si Schottky barrier diodes, Journal of Materials Science: Materials in Electronics, 29 (2018) 2618-2627.
[56] A. Buyukbas-Uluşan, S.A. Yerişkin, A. Tataroğlu, M. Balbaşı, Y.A. Kalandaragh, Electrical and impedance properties of MPS structure based on (Cu 2 O–CuO–PVA) interfacial layer, Journal of Materials Science: Materials in Electronics, 29 (2018) 8234-8243.
[57] A.B. Uluşan, A. Tataroğlu, Y. Azizian-Kalandaragh, Ş. Altındal, On the conduction mechanisms of Au/(Cu 2 O–CuO–PVA)/n-Si (MPS) Schottky barrier diodes (SBDs) using current–voltage–temperature (I–V–T) characteristics, Journal of Materials Science: Materials in Electronics, 29 (2018) 159-170.
[58] A. Tataroğlu, Ş. Altındal, The analysis of the series resistance and interface states of MIS Schottky diodes at high temperatures using I–V characteristics, Journal of Alloys and Compounds, 484 (2009) 405-409.
[59] S.S. Li, Semiconductor physical electronics, Springer Science & Business Media, 2012.
[60] H. Tecimer, Ş. Altındal, S. Aksu, Y. Atasoy, E. Bacaksız, Interpretation of barrier height inhomogeneities in Au/In 2 S 3/SnO 2/(In-Ga) structures at low temperatures, Journal of Materials Science: Materials in Electronics, 28 (2017) 7501-7508.
[61] T.E.C. Jr., C.C. Fulton, W.J. Mecouch, K.M. Tracy, R.F. Davis, E.H. Hurt, G. Lucovsky, R.J. Nemanich, Measurement of the band offsets of SiO2 on clean n- and p-type GaN(0001), Journal of Applied Physics, 93 (2003) 3995-4004.
[62] T. Cook Jr, C. Fulton, W. Mecouch, R. Davis, G. Lucovsky, R. Nemanich, Band offset measurements of the Si 3 N 4/GaN (0001) interface, Journal of applied physics, 94 (2003) 3949-3954.
[63] Ş. Aydoğan, K. Çınar, H. Asıl, C. Coşkun, A. Türüt, Electrical characterization of Au/n-ZnO Schottky contacts on n-Si, Journal of Alloys and Compounds, 476 (2009) 913-918.
[64] W. Hill, C. Coleman, A single-frequency approximation for interface-state density determination, Solid-State Electronics, 23 (1980) 987-993.
[65] A. Turut, Determination of barrier height temperature coefficient by Norde's method in ideal Co/n-GaAs Schottky contacts, Turkish Journal of Physics, 36 (2012) 235-244.
[66] A. Turut, A. Karabulut, H. Efeoglu, Electrical characteristics of atomic layer deposited Au/Ti/Al2O3/n-GaAs MIS structures over a wide measurement temperature, JOURNAL OF OPTOELECTRONICS AND ADVANCED MATERIALS, cilt.19 (2017) 424-433.
[67] K. Ejderha, S. Asubay, N. Yildirim, Ö. Güllü, A. Turut, B. Abay, The characteristic diode parameters in Ti/p-InP contacts prepared by DC sputtering and evaporation processes over a wide measurement temperature, Surface Review and Letters, 24 (2017) 1750052.

[68] A. Karabulut, I. Orak, M. Caglar, A. Turut, THE CURRENT–VOLTAGE CHARACTERISTICS OVER THE MEASUREMENT TEMPERATURE OF 60–400 K IN THE Au/Ti/n-GaAs CONTACTS WITH HIGH DIELECTRIC HfO2 INTERFACIAL LAYER, Surface Review and Letters, 26 (2019) 1950045.
[69] A. Karabulut, H. Efeoglu, A. Turut, Influence of Al2O3barrier on the interfacial electronic structure of Au/Ti/n-GaAs structures, Journal of Semiconductors, 38 (2017) 054003.

Figure captions

Fig. 1 XRD of SnO_2 thin films with various concentrations of Zr dopant.

Fig. 2 FE-SEM images of SnO_2 thin films with different concentration of Zr. (a) SnO_2, (b) Zr(2 wt.%):SnO_2, (c) Zr(4 wt.%):SnO_2, (d) Zr(6 wt.%):SnO_2, (e) Zr(8 wt.%):SnO_2 and (f) EDAX spectra of Zr(8 wt.%):SnO_2 thin film.

Fig. 3 (a) Optical absorbance spectra and (b) Tauc's $[(\alpha h\nu)^{1/2}$ vs. $h\nu]$ plot of Zr:SnO_2 thin films.

Fig. 4 Temperature dependence of electrical conductivity of the Zr-doped SnO_2 thin films. (a) SnO_2, (b) Zr(2 wt.%):SnO_2, (c) Zr(4 wt.%):SnO_2 and (d) Zr(6 wt.%):SnO_2.

Fig. 5 Plot of $\ln(\sigma_{dc})$ vs. 1/T of the SnO_2 thin films for different dopant concentration of Zr. (a) SnO_2, (b) Zr(2 wt.%):SnO_2, (c) Zr(4 wt.%):SnO_2 and (d) Zr(6 wt.%):SnO_2.

Fig. 6 Plot of ln(I) vs. V of the SnO_2 thin films for various dopants of Zr in the Al/ Zr:SnO_2/p-Si.

Fig. 7. Metal-p-type semiconductor contact a) Before contact, b) Thermal equilibrium after contact c) under forward bias d) under reverse bias conditions.

Fig. 8 (a) plot of dV/dIn(I) versus I and (b) H(I) versus I for various dopants of Zr.

Declaration of interests

☒ The authors declare that they have no known competing financial interests or personal relationships that could have appeared to influence the work reported in this paper.

☐The authors declare the following financial interests/personal relationships which may be considered as potential competing interests: